# An Evaluation of the use of a Multibeam Echo-Sounder for Observations of Suspended Sediment

Stephen M. Simmons[a], Daniel R. Parsons[a], James L. Best[b], Kevin A. Oberg[c], Jonathan A. Czuba[d] and Gareth M. Keevil[e]

[a]School of Environmental Sciences, University of Hull, Cottingham Road, Hull, HU6 7RX, #UK

[b]Departments of Geology, Geography GIS, Mechanical Science and Engineering & Ven Te Chow Hydrosystems Laboratory, University of Illinois, 605 West Springfield Avenue, Champaign, IL 61820, USA

[c]U.S. Geological Survey, Office of Surface Water, 1201 W. University Ave, Suite 100, Urbana, IL 61801, USA

[d]Department of Civil, Environmental, and Geo- Engineering and St. Anthony Falls Laboratory, University of Minnesota, 2 Third Ave SE, Minneapolis, MN 55414

[e]School of Earth and Environment, University of Leeds, Leeds LS2 9JT, UK

**Corresponding author: Stephen Simmons, s.simmons@hull.ac.uk**

**Abstract**

The theory relating the acoustic backscatter from suspended sediments to the mass concentration of particles has been developed over several decades and is now routinely applied to provide measurements for commercial and scientific applications. Single-beam instruments, such as acoustic Doppler current profilers (ADCP), permit acquisition of backscatter along one-dimensional spatial profiles. However, commercially available multibeam echo-sounders (MBES), designed principally for bathymetric surveying, now offer water column backscatter data-logging across their two-dimensional interrogation swaths, enabling suspended sediment to be instantaneously imaged across much larger volumes. This paper addresses issues relating to the processing of suspended sediment backscatter recorded with an MBES system, drawing on the theory developed for single-beam instruments. A processing methodology is developed and the performance limits estimated from an analysis of the data acquired in the near-field of a Teledyne-RESON MBES in a controlled test facility. Results derived from the application of the methodology to field-data collected with an MBES and an ADCP in the Missouri River, USA, are presented that demonstrate the potential gains in spatial and temporal resolution and near-bed imaging than can be achieved by the use of an MBES system.

**Keywords**: Multibeam, Suspended Sediment

## 1. INTRODUCTION

The inversion of acoustic suspended sediment backscatter to determine concentration is a well-established field of study (see Thorne and Hurther, 2014) and a range of acoustic instruments are now routinely deployed for the measurement of suspended sediment concentration (SSC) in fluvial (e.g. Lane et al., 2008; Simmons et al., 2010; Shugar et al., 2010; Best et al., 2010; Latosinski et al. 2014), estuarine (e.g. Thorne et al., 1993; Holdaway et al., 1999), lacustrine (e.g. Best et al., 2005) and coastal environments (e.g. Thorne et al., 2007). The approach has the advantage of being non-intrusive and transducers are capable of acquiring data along profiles with high spatial resolution over ranges of less than 1 m for near-bed measurements to 25 m in the marine environment (see Thorne and Hurther, 2014). Instruments can facilitate the concurrent measurement of bed morphology and hydrodynamics (e.g. Traykovski et al., 1999), both of which are inter-connected with the SSC in the water column (Leeder, 1983; Best, 1993); the measurement of all three facets thus provides a greater insight into the process dynamics of sedimentary regimes.

Commercially available single-frequency acoustic Doppler current profilers (ADCP) have frequently been used to obtain SSC profiles by mounting the instrument on static frames above the bed (e.g. Holdaway et al., 1999) and by deployment from a survey vessel (e.g. Lane et al., 2008; Shugar et al., 2010, Latosinski et al. 2014). ADCPs have the advantage that SSC profiles and three-dimensional velocity data can be simultaneously acquired (e.g. Lane et al., 2008; Shugar et al., 2010). Although it is possible to quantify the sediment transport flux in a river by collecting ADCP data along a transect line, the angle of incidence of the ADCP beams with the bed leads to the presence of side-lobe interference in the near-bed cells, thus causing errors in the SSC measurements (Vincent, 2007).

The backscatter magnitude from a suspension of sediment is a function of the grain size in suspension as well as the mass concentration (mg/L), and instruments that typically operate on lower frequencies, such as ADCP and multibeam echo-sounders (MBES), can be very sensitive to changes in the grain size when operating in the Rayleigh scattering regime with $ka \ll 1$, where $k$ is the acoustic wave number and $a$ is the suspended sediment particle radius. Acoustic backscatter (ABS) instruments have been developed (see Thorne and Hurther, 2014) that use higher frequencies in the range 0.5 MHz to 5 MHz and are less sensitive to grain size variations. By acquiring data on multiple frequencies, the mean grain size can be determined by comparing the ratios of the backscatter to derive concentration values without the need to calibrate to water column samples. However, these systems are usually deployed on a static frame near the bed for study of smaller-scale sediment processes (e.g. Thorne et al., 2007).

MBES systems have been available commercially for many years and are routinely deployed on survey vessels to provide high-resolution bathymetric mapping (e.g. Czuba et al., 2011; Flood et al., 2009; Lane et al., 2008; Parsons et al., 2005; Parsons et al., 2010). In early systems, the scattering data from the water column was discarded after the range to the bed had been determined for each beam in the swath. However, with the advent of greater processing power and data storage technology, some MBES systems now provide the option to record the large quantities of water column backscatter data. This facility has benefitted applications including the study of fish populations, marine mammals, zooplankton, kelp ecosystems, aquaculture, near-surface bubbles, gas venting and marine archaeology (see Colbo et al., 2014). The application of MBES for the imaging of suspended sediment was first realized during the bathymetric surveying of a dune-field at the confluence of the Rio Paraná and Paraguay, with the first quantitative SSC results derived by the application of the sonar equation and calibration to water column SSC samples being presented by Simmons et al. (2010). The technique has further been applied to quantify the volume and sediment load of plumes entrained from the sea bed by the action of commercial trawler gear (O'Neill et al., 2013). MBES has the advantage over single-beam acoustic instruments of providing information across a two-dimensional swath, readily providing instantaneous images of suspended sediment structures. MBES also provides high-resolution bathymetry and when deployed at a fixed point, two-dimensional velocity vectors can be obtained by correlating the processed backscatter in successive pings (Best et al., 2010; Simmons et al., 2008). As such, MBES provides a means by which the three inter-related process of sediment transport — concentration, bed-morphology, and hydrodynamics — may be measured concurrently over a two-dimensional interrogation area. Additionally, the roughness of the bed can also be estimated from the backscatter (e.g. Fonseca and Mayer, 2007). Although the near-bed regions of the MBES backscatter swath that are free from side-lobe interference are limited in horizontal extent, by locating the beam with the shortest range to the bed it is possible to obtain near-bed backscatter data without the specular side-lobe contamination associated with ADCP instruments that occurs as a result of the grazing angle of the beams with the bed.

This paper presents water column backscatter MBES results obtained from a series of directed and systematically-controlled tests of the system in a large-scale experimental basin facility. The test results demonstrate the ability of MBES to successfully image known concentrations of suspended material in the near-field. Estimates of the imaging range of the technique for different sedimentary regimes are also presented. The results and analysis of a field deployment of the same MBES system, deployed above a fluvial sand-dune, are subsequently detailed and compared with results obtained with an ADCP at the same location.

## 2. THEORY

The work reported herein utilises a demonstration model of the Teledyne-RESON SeaBat 7125 MBES. The system produces a wide fan of beams across an arc of $128^0$ that interrogates a narrow slice of the water column at ping repetition frequencies of up to 50 Hz. The Teledyne-RESON SeaBat 7125 MBES can be operated on a frequency of either 200 kHz with 256 electronically-formed beams, or at 396 kHz with a choice of 256 or 512 electronically formed beams. There are two beamforming modes of operation, which result either in equi-angular or equi-distant beam-spacing across the 128 degree arc. The TC2163 (200 kHz) and TC2160 (396 kHz) transmitter ceramic arrays are aligned orthogonally to the receiver ceramic array in a Mills Cross configuration (Mills and Little, 1953) and can be seen mounted and ready for deployment in the calibration tank in Figure 1. The combined directivity patterns of the transmitter and receiver result in a -3dB main-lobe along-track beamwidth specified as $2.2^0$ at 200 kHz and $1.0^0$ at 396 kHz and an across-track broadside beamwidth of $1.1^0$ at 200 kHz and $0.54^0$ at 396 kHz. The pulse length can be varied between 30 μs and 300 μs and the transmitter power from 170 to 220, reported as dB re: 1 μPa at 1 m. The system gain is the sum of the user-defined fixed gain, $G_{R,}$ (0 to

83 range) and time-varying gain (TVG), $G_{TVG}$, which is a function of the absorption loss value (0 to 120 range) and spreading loss coefficient (0 to 60 range). The TVG function is non-standard and not publically available, however the spreading term can be described as logarithmic and the frequency-dependant absorption-term as linear and are designed to maintain the signal level at the receiver within the dynamic range of the system (Schimel et al., 2015). The sample rate is fixed at 34,483 Hz corresponding to a sampling interval of 29 μs and, consequently, sampling volumes overlap for pulse lengths greater than 29 μs, resulting in a loss of independence between adjacent sampling volumes. The maximum range setting is 500 m at 200 kHz and 300 m at 396 kHz. The data presented herein were acquired using the standard continuous wave setting. Dynamic focusing of the receiver array beyond a range of 1.5 m is designed to mitigate the near-field effects, however, the transmitter array is unfocused and, at a length of 0.196 m, has a near-field extending to ~10 m at 200 kHz and ~20 m at 396 kHz.

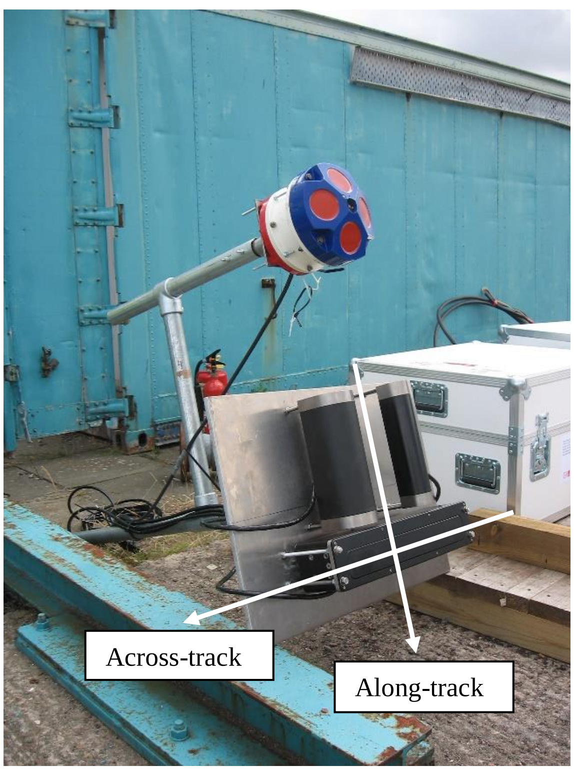

Figure 1. Teledyne-RESON SeaBat 7125 transducers prior to deployment in the calibration tank. The black transducer arrays are mounted on a rigid plate. An ADCP is also mounted separately on a scaffold pole to the rear of 7125 transducers.

For low concentrations of SSC where multiple scattering is assumed to be negligible (<10 g/L), the mass concentration of particles per unit volume, $M$, is related (Sheng and Hay, 1988; Thorne and Hurther, 2014) to the root mean square value of the backscatter magnitude recorded by the receiver, $B_{\mathrm{rms}}$, thus:

$$M = \left( \frac{B_{\mathrm{rms}} r \psi_b}{S K_{\mathrm{t},b} K_{\mathrm{s}}} \right)^2 e^{4(\alpha_{\mathrm{w}} + \alpha_{\mathrm{s}})r} \quad (1)$$

where $r$ is the range from the receiver array face, $\psi_b$ is a near-field correction for the $b^{\mathrm{th}}$ beam as function of the range from the transducers, $K_{\mathrm{t},b}$ is a constant for each beam and relates the linear relationship between the sound pressure at the receive array and the recorded backscatter magnitude, $B$ (counts), and is a function of the volume integration of the transmitter and the receiver array directivities and receiver sensitivity. The backscatter magnitude recorded by the SeaBat 7125 is proportional to the pressure at the transducer face. $K_{\mathrm{s}}$ is a property of the particles and their size distribution in suspension, $\alpha_{\mathrm{w}}$ and $\alpha_{\mathrm{s}}$ are the attenuation terms related to the properties of the water and suspended sediment respectively, $S$ is a function of the transmitter pulse length, $\tau$, the transmitter power setting, $P_{\mathrm{T}}$ (dB), and the system gain as a function of $r$:

$$S = \tau^{1/2} 10^{\frac{P_{\mathrm{T}} + G_{\mathrm{R}} + G_{\mathrm{TVG}}}{20}} \quad (2)$$

$K_{\mathrm{S}}$ is determined by:

$$K_{\mathrm{S}} = \frac{f_{\mathrm{e}}}{\sqrt{\bar{a}\rho}} \quad (3)$$

where $a$ is the particle radius, ρ is the density of the grain material and $f_e$ is the ensemble form function of the particle size distribution describing the backscattering properties of the particles relative to their geometric size. $K_S$ is therefore a function of the suspended sediment type and grain size distribution and can only be assumed constant if the properties of the sediment in suspension remain constant. The clear water sound attenuation, $\alpha_{w,}$ can be determined using commonly deployed formulae (Francois and Garrison, 1982a and 1982b, used herein). The sediment attenuation, $\alpha_s$, is determined by integrating the product of the sum of the ensemble scattering and viscous absorption attenuation coefficients, $\zeta = \left(\zeta_{\text{scat}}(k\bar{a}) + \zeta_{\text{visc}}(k\bar{a})\right)$, and the mass concentration, $M$, along the propagation path:

$$\alpha_s = \frac{1}{r}\int_0^r \zeta M dr \qquad (4)$$

$\zeta_{\text{scat}}(k\bar{a})$ is determined (following Sheng and Hay, 1988) by

$$\zeta_{\text{scat}}(k\bar{a}) = \frac{3M\chi_e(k\bar{a})}{4\bar{a}\rho} \qquad (5)$$

where $\chi_e$ is the ensemble normalised total scattering cross-section, which describes the total scattering of the particle size distribution relative to its geometric cross section. The formulae of Urick (1948) is used herein to calculate $\zeta_{\text{visc}}(k\bar{a})$ using assumed values of kinematic viscosity and the density of the grain material in suspension.

Heuristic expressions have been developed by previous researchers (e.g. Moate and Thorne, 2012; Sheng and Hay, 1988; Thorne et al., 1993) to describe the form function and scattering cross-section algebraically, by fitting a high-pass model to a combination of measured data and physical models of acoustic scattering by spheres. The expressions are based on the dimensionless relationship between the acoustic wave number and the particle size, $ka$, with asymptotes for the scattering regimes far from $ka=1$, with $f$ proportional to

$(ka)^2$ and $\chi$ proportional to $(ka)^4$ for the Rayleigh scattering regime ($ka$<<1), and with $f$ and $\chi$ constant for the geometric scattering regime ($ka$>>1). The expressions are fitted to empirical data in the transition between the two regimes. For the Teledyne-RESON SeaBat 7125 frequencies, $ka$ is unity at $a$ = 1.2 mm at 200 kHz and $a$ = 0.59 mm at 396 kHz for a nominal sound speed of 1480 m/s. The backscatter for the majority of naturally-occurring suspended sediments will hence lie within the Rayleigh scattering regime.

Solving Eq. (1), to yield a value of mass concentration from the backscatter magnitude, requires a knowledge of the grain size distribution and calibration constants, $K_{t,b}$. Additionally, the sediment attenuation, $\alpha_s$, is itself a function of $M$. If the expected values of concentration and grain size in suspension cause $\alpha_s$ to be relatively small over the propagation path, then it may be approximated to zero, thus enabling Eq. (1) to be solved directly. If $\alpha_s$ is significant, then an iterative approach based on an implicit solution to Eq. (1) may be employed to form successive estimates of $M$. The first estimate of $M$ is found by setting $\alpha_s$ to zero in Eq. (1), which is then used to determine $\alpha_s$, and subsequently update the value of $M$ and then $\alpha_s$ through a number of iterations until $M$ converges (e.g. Thorne et al., 1993). However, care is needed as errors may accumulate in a positive feedback loop as the solution is evaluated along the propagation path (see Thorne et al., 2011).

The random distribution of particles within the sampling volumes leads to a random, uniform, distribution of backscatter phase and a random, Rayleigh distribution of backscatter magnitude, $B$, for successive ensonifications of the same volume (Hay et al., 1983; Libicki et al., 1989; Thorne, 1993). Spatial or temporal averaging of the data thus reduces the expected error of the mass concentration value, *M*, derived using Eq. (1), at the expense of resolution. The percentage relative standard error (RSE) of the averaged backscatter, $B_{\mathrm{rms}}^2$, is related to the number of independent samples, *N*, by (Libicki et al., 1989):

$$RSE(B_{\mathrm{rms}}^2) = \frac{100}{\sqrt{N}} \quad (6)$$

ABS processing methods conventionally average the backscatter values between successive profiles to derive a value of $B_{\mathrm{rms}}$. However, the large quantity of backscatter data available in the two-dimensional swath of a single MBES ping enables sufficient averaging to be performed over local areas of a single ping for the relative standard error to reduce to acceptable levels. A two-dimensional spatial averaging method for MBES data has been described previously for data collected in the field with a Teledyne-RESON 8125 MBES (Simmons et al., 2010). The same method of allocating the average of the samples within a specified radius to the central sample is applied herein to data collected with the Teledyne-RESON SeaBat 7125. As the data is averaged over an area, rather than through time for a single sample, the method applies the range, attenuation, system settings and constant terms in Eq. (1) prior to averaging and before squaring to derive *M*.

The quoted main-lobe beamwidths and beam spacing for the SeaBat 7125 MBES imply that adjacent beams will overlap one another, leading to spatial oversampling, in addition to the oversampling that occurs along the radial distance from the transducers when the pulse length exceeds 29 μs. The -3dB across-track main-lobe beamwidth at broadside is quoted as $1.0^0$ at 200 kHz and $0.5^0$ at 396 kHz. However, the effective aperture is expected to increase with steering angle from broadside, with the beamwidth of the $b^{\text{th}}$ beam, $\vartheta_b$, defined as:

$$\vartheta_b = \vartheta_{\text{broadside}} / \cos(\theta_b) \tag{7}$$

where $\theta_b$ is the steering angle of the $b^{\text{th}}$ beam's main-lobe. Thus, the across-track beamwidth is ~$2.28^0$ at 200 kHz and ~$1.14^0$ at 396 kHz for the beams farthest from broadside. There are two modes of operation in the Teledyne-RESON SeaBat 7125 MBES: equi-angular, with equal angular spacing between adjacent beams, and equi-distant, where the angle varies to provide equal horizontal spacing between the reflections from a flat bed. The largest overlap between adjacent beams occurs in equi-distant mode for the farthest beams, and is estimated to be ~93% for both the 256 beams setting at 200 kHz and 512 beams setting at 396 kHz. The maximum overlap along a beam, ~90%, occurs at the maximum pulse length setting of 300 μs. When sampling volumes overlap, the relative standard error will be greater than that described by Eq. (6).

Dynamic focusing is applied to the receive array beyond a range of 1.5 m, and thus any near-field effects are considered to be dominated by the transmit arrays. The array of ring transducers of the transmit units will produce a -3 dB beamwidth that is approximately equal to the 200 mm length of the array in the along-track axis within the near-field. The sampling volumes within the near-field are therefore wider in the along-track axis than if the far-field beamwidths of $2.2^0$ at 200 kHz and $1.0^0$ at 396 kHz are used to determine the sampling volume. However, the apparent source level at ranges within the near-field are likely to be lower than the level expected if the far-field spreading relationship with range was extended to the near-field.

# 3. EXPERIMENTAL TESTS

## Experimental Setup

Large-scale basin testing of the MBES was undertaken at the New and Renewable Energy Centre (NaREC) Ark Royal site, on the Blyth Estuary, Northumberland, UK. The basin consisted of a former dry-dock, measuring approximately 100 m × 19 m × 6 m, which was filled by pumping the adjacent estuary water on the flood-tide. An aluminium square truss (lighting-truss) was assembled to span the width of the basin, with the MBES mounted rigidly on a bracket attached to a pole suspended below the centre of the truss (Fig. 1).

Backscatter data were recorded with the MBES whilst known quantities of wetted sediment were released via a vertical section of pipe, with an internal diameter of 63 mm, positioned ~1.5 m along the truss from the MBES mounting pole. The outlet of the pipe was located ~1.2 m below the depth of the transducers and was aligned with the MBES acoustic interrogation volume to facilitate the recording of backscatter from the resulting gravity plume. Weighed quantities of sand-sized glass spheres, with a $D_{50}$ value of 267.5 μm and a mean grain radius, $a_{mean}$, of 115.7 μm, were released during the tests; these were prepared by prior mixing with water, to reduce the entrainment of air bubbles, and were released manually into a funnel connected to the pipe. Quantities of 7 g / 14 g / 70 g / 140 g / 400 g / 200 g / 1000 g were weighed prior to release and backscatter data were acquired with the MBES whilst the plumes of material were observed to descend to the bed.

## Observations and Analysis: Suspended Sediment

The magnitudes of the backscatter from all the plumes were visibly greater than the background acoustic noise for all quantities of material released. Figure 2 shows typical plume backscatter magnitudes resulting from the release of 1 kg of the sand-sized glass spheres. The outlet of the pipe is at a location approximately 1.2 m below the transducer array surface and -1.5 m across track. The MBES mounting pole had a slight angle to the vertical, resulting in the slanted appearance of the bed echoes. A nadir noise artefact is visible at broadside. The backscatter from the plume is clearly visible, extending to a depth below the transducers of ~4 m in two distinct structures and with material appearing to be still descending from below the pipe. Backscatter from the descending plumes were recorded over a period of three days on different settings of transmitter power, receiver gain and pulse length, but all with a TVG spreading coefficient of 10 dB and a ping repetition frequency of 10 Hz. Higher repetition frequencies were found to result in noticeable surface reverberation effects. The mean water temperature throughout the tests was measured as $13.1^0$ C which, when combined with an assumed salinity of 35 ppt, pH of 8 and depth of 5 m, results in a derived value of water attenuation of $\alpha_w$ = 0.007 Np / m at 200 kHz and $\alpha_w$ = 0.012 Np / m at 396 kHz using the formulae of Francois and Garrison (1982a and 1982b).

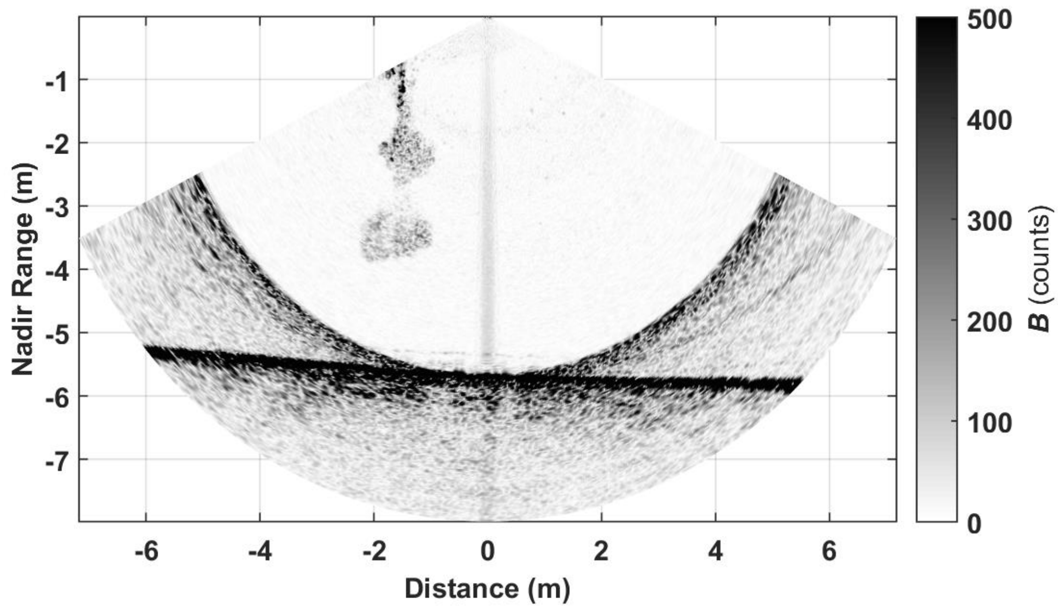


Figure 2 - Magnitude data from a single ping recorded in the test basin at 396 kHz (512 equi-angle beams), showing the backscatter from the plume of 1 kg of sand-sized glass spheres. $P_T$ = 190 dB, $G_R$ = 45 dB, $\tau$ = 60 μs. Magnitude values are clipped above a magnitude of 500 counts to improve the contrast with the bed.

The plume analysis method presented herein was developed to quantify the calibration constant by relating the quantity of material released through the pipe to the cumulative backscatter from an estimate of the three-dimensional volume of the plumes. The method is derived from the implicit iterative approach (see Thorne and Hurther, 2014) to evaluate Eq. (1). The swath calibration constant, $K_{t,swath}$, is hence described as:

$$K_{t,swath} = \frac{\pi}{\sqrt{\Pi}} \int_{z_{min}}^{z_{max}} \int_{x_{min}}^{x_{max}} \left( \frac{B_{rms} r \psi_b}{S K_S} \right) e^{2(\alpha_w + \alpha_s) r} x dx dz \tag{8}$$

where $\Pi$ (kg) is the quantity of material released through the pipe. At present, no expression exists for the near-field correction, $\psi_b$, which is therefore set to unity on the assumption that the increase in beamwidth within the near-field is likely to be offset by the reduction in the apparent source level. $x$ is the across track coordinate (see Fig. 1) and $z$ is the vertical coordinate, i.e. the depth below the transducers, of the cylindrical coordinate system. A necessary assumption is made that the value of $K_{t,b}$ does not vary across the swath, hence the constant is described as $K_{t,swath}$ for all beams. The cylindrical coordinate system of the integral necessitates a two-dimensional interpolation of the processed MBES swath backscatter data to a Cartesian grid.

First, a range of pings for each plume is manually selected to ensure the full volume of the plume is visible between the pipe outlet and the farthest range of the swath above the arc formed by the specular echoes from the bed. An estimate of $B_{corrected}$, the backscatter corrected for spreading, water attenuation, the sonar settings and $K_S$, is then obtained with:

$$B_{corrected} = \left( \frac{B_{rms} r}{S K_S} \right) e^{2\alpha_w r} \tag{9}$$

with $K_S$ determined using the ensemble form function the formulae of Gaunaurd and Uberall (1983) for scattering from elastic spheres and the grain size distribution of the sand-sized glass spheres obtained with a Malvern Mastersizer 2000e laser-diffraction grain sizer in 1/5 φ size bins. The temporal RMS of the backscatter data is evaluated over a period of up to 10 s before the lower extent of the plume reaches the bed. The two-dimensional polar data is then interpolated onto a Cartesian grid in the $x$ and $z$ coordinates with a resolution of 0.1 m and the area of the plume within the swath determined as the backscatter greater than 6 dB above the background noise. The centre of each horizontal segment of plume data is determined and the averaged values of $B_{\text{corrected}}$ within the segment are multiplied by the volumes formed by the rotation of the swath image about the centre. The Cartesian limits of the integral of Eq. (8) are thus determined by the backscatter magnitude and the rotation of the 2D plume image, giving a 3D plume volume bounded by the *x* and *z* coordinate limits manually chosen for each plume. The first estimate of the calibration constant, $K_{\text{t,swath}}$, is derived from the evaluation of the integral of the 3D plume volume using Eq. (8) with $\alpha_s$=0. A first estimate of concentration, *M*, across the 2D swath is calculated using the calibration constant with the averaged value of $B_{\text{corrected}}$:

$$M = \left( \frac{\overline{B_{\text{corrected}}}}{K_{\text{t,swath}}} \right)^2 e^{4(\alpha_{\text{w}} + \alpha_{\text{s}})r} \tag{10}$$

The first estimate of $\alpha_s$ is found by multiplying *M* by the sediment attenuation coefficient [Eq. (4)], derived using the scattering cross-section expression of Gaunaurd and Uberall (1983) and the viscous absorption expression of Urick (1948) using the measured grain size distribution with a glass sphere material density of 2500 kg/m$^3$, as quoted by the manufacturers, and a value of kinematic viscosity of 1.2 × 10$^{-6}$ m$^2$/s based on the mean recorded temperature of 13.1$^0$ C and the description provided by Kestin et al. (1978). The sediment attenuation, $\alpha_s$, is then used to update the concentration estimate and the same process was iterated ten times. The values of *M* across the two-dimensional swath are then interpolated to a Cartesian grid with the total mass of material in the plume, $\Pi'$, estimated in the same manner as the method to determine the first estimate of $K_{\text{t,swath}}$. The difference between $\Pi'$ and the mass released through the pipe, $\Pi$, is then used to update the estimate of $K_{\text{t,swath}}$. The process is then iterated several times until two consecutive values of $K_{\text{t,swath}}$ differ by less than 0.01%.

Figure 3 shows the results of the basin tests with least-squares fit through the origin for the 396 kHz data (solid) and for the 200 kHz data (dashed) using the plume backscatter volume integration. The y-axis describes the implied values of $\Pi^{1/2} K_{t,swath}$ derived using the volume integration term of Eq. 8 and the x-axis is the square root of the quantity of material released in to suspension, $\Pi^{1/2}$. The slope of the least square fits gives a value of $K_{t,swath} = 6.55 \times 10^{-7}$ counts $m^{3/2}\ s^{-1/2}$ at 200 kHz and $K_{t,swath} = 6.31 \times 10^{-7}$ counts $m^{3/2}\ s^{-1/2}$ at 396 kHz.

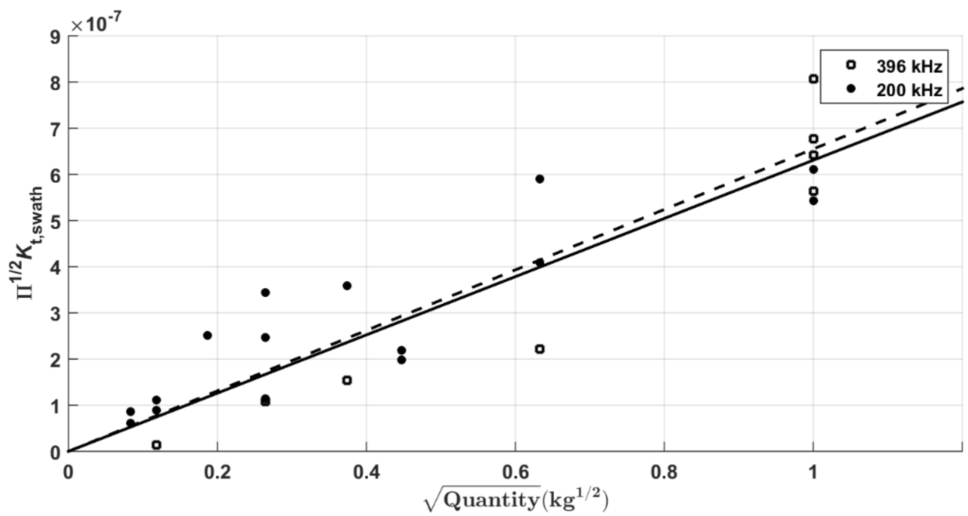


Figure 3 – Least-square linear calibrations of the data from the basin tests at 200 kHz and 396 kHz.

The value of $K_{t,swath} = 6.31 \times 10^{-7}$ counts $m^{3/2}\ s^{-1/2}$ for the 396 kHz frequency compares with a value of $1.51 \times 10^{-6}$ counts $m^{3/2}\ s^{-1/2}$ obtained by O'Neill et al. (2013) using another SeaBat 7125 system that was used to record backscatter from a plume of suspended sediment entrained by demersal trawling gear that was calibrated to concentration values measured with a Laser In-situ Scattering and Transmissometer (LISST) positioned in the plumes by divers. Greenaway and Weber (2010) measured the individual ceramic element sound pressure level response of a SeaBat 7125 system using a calibration tank and hydrophones that transmitted towards the receiver array. They measured the system gain, defined as the combined hydrophone sensitivity and fixed gains that relate the pressure at the transducer face to the magnitude values recorded by the instrument in counts, as -121 dB at 200 kHz and -113 dB at 396 kHz for the linear range of the receiver. Greenaway and Weber (2010) also measured the beam-formed magnitude response at 200 kHz using a calibration sphere of unknown target strength and at 396 kHz using the bed-echo backscatter collected in the field with several SeaBat 7125 systems and found an additional beam-former gain of 5.8 dB at 200 kHz and between 3.5 dB and 7.0 dB at 396 kHz. Combining the measured system responses and beam former gains measured by Greenaway and Weber (2010) with the -3 dB beamwidths, yields approximate values of $K_{t,swath} = 3 \times 10^{-7}$ counts $m^{3/2}$ $s^{-1/2}$ at 200 kHz and $3 \times 10^{-7}$ counts $m^{3/2}$ $s^{-1/2}$ at 396 kHz that are lower than the values presented herein. However, the study of the variability of the power, gain and pulse length settings between three different SeaBat 7125 units by Welton (2014) suggests that such differences could be due to deviations from the ideal relationships rather than actual direct measurement error.

With the aim of estimating the concentration and grain size of sediment that the SeaBat 7125 MBES system is capable of imaging, a model of the backscatter was produced by re-arranging Eq. (1) to give an expression for $B_{rms}$. The model is based on the maximum pulse length of 300 μs and assumes that SSC is homogeneous throughout the range and that the grain size distribution is log-normal with a relative standard deviation of 0.3. The range is defined as the distance to which the backscatter magnitude drops below a threshold, defined as being equal to the expected magnitude of noise (0 dB signal-to-noise ratio) with the receiver gain at the maximum value of 83 dB. The average system noise magnitude acquired with a gain of 83 dB at the test facility with a mean temperature of $13.1^{0}$ was 79.7 counts at 200 kHz and 278.7 counts at 396 kHz, although it should be noted that these values will likely vary between systems and are dependent on temperature. Figure 4(a) shows the results from the 200 kHz model with $K_{t,swath} = 6.55 \times 10^{-7}$ counts $m^{3/2}$ $s^{-1/2}$. The range increases with mean grain size and concentration and reaches the maximum range of around 380 m. However, on the right-hand side of the plot, increased sediment attenuation limits the range. Figure 4(b) shows the results from the 396 kHz model with $K_{t,swath}$=$6.31 \times 10^{-7}$ counts $m^{3/2}$ $s^{-1/2}$. The pattern is similar to 200 kHz, but the maximum range is higher and reaches the maximum of 500 m as a result of the higher values of *ka* and form function.

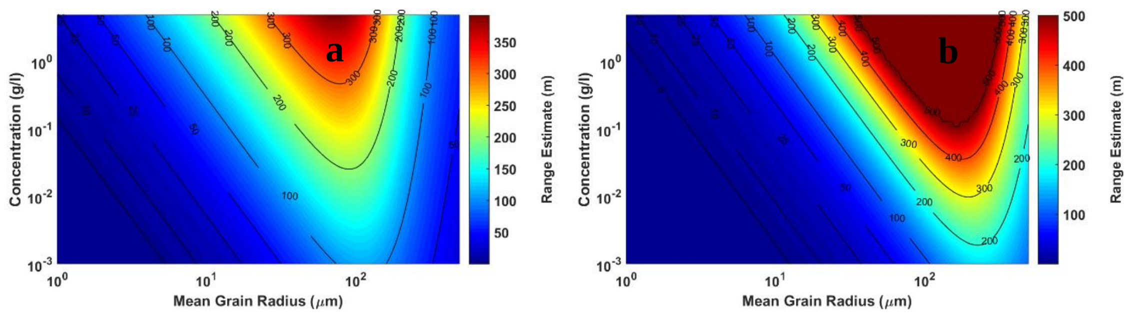


Figure 4 – Estimated range at (a) 200 kHz and (b) 396 kHz for which the mean backscatter magnitude of the broadside beams drops to a signal-to-noise ratio of 0 dB, for homogeneous concentrations of suspended sediment with a log-normal distribution and with a relative standard deviation of 0.3.

## 4. FIELD TESTS

### Experimental Setup

Measurements of sediment transport over the leeside of an alluvial sand-dune were undertaken during a survey of a reach of the Missouri River, USA, at a location ($38^0$ 49.314150' N, $90^0$ 10.114794' W) upstream of the confluence with the Mississippi River. The survey vessel was held at a stationary position with a three-point anchor whilst acoustic backscatter data were collected using the same MBES system that was deployed for the basin tests and also with a Teledyne-RDI 1200 kHz ADCP. The MBES transducers were mounted at the bow with the swath aligned parallel to the direction of river flow at a depth of 0.3 m below the flow surface. The ADCP was mounted from the side of the vessel at the same depth below the surface, with a lateral and downstream offset of the ADCP from the MBES of 1.25 m and 0.79 m respectively. A P61 point-integrating water sampler (see Guy and Norman, 1970) was deployed to collect suspended sediment samples at discrete heights above the bed. The beginning and end of each sample collection was controlled by the P61's electrically operated valve. The depth to the bed was typically ~7 m and the bed morphology was characterized by a field of sand dunes with asymmetrical profiles comprising steeper downstream lee slopes and shallower upstream stoss slopes. The boat was moored over the leeside of one of these dunes with a trough to crest elevation of ~ 0.9 m.

To calibrate the acoustic data, seven P61 samples were obtained at depths of 3.5 m / 4.5 m / 5.0 m / 5.5 m / 6.0 m / 6.5 m / 6.8 m whilst the MBES simultaneously recorded backscatter over periods of up to 20 s for each sample. The pulse repetition frequency was set to 10 Hz in equi-angle mode at 396 kHz with 512 beams and with $P_T$ = 200 dB, $G_R$ = 58 dB, $\tau$ = 49 μs, $G_{spreading}$ = 30 dB and $G_{absorption}$=50 dB/km. A longer continuous sequence of MBES backscatter data were acquired with the same settings over a period of ~7 minutes and, to provide a comparison between the spatial and temporal resolution of the MBES and ADCP, a ~40 minutes sequence of ADCP data was also acquired. The ADCP cell size was equivalent to 0.2 m in the vertical and the profiles for each of the four beams at 20 degrees to the vertical were acquired at a pulse repetition frequency of 10 Hz and were averaged internally over 6 successive profiles.

## Observations and Analysis

The P61 water column samples were filtered and weighed in to two size fractions greater and less than 62.5 μm diameter. Using the approximation, $\alpha_S = 0$, based on an assumed low value of sediment attenuation, the following expression is derived from Eq. 1 for the calibration:

$$MK_S^2 K_{t,\mathrm{broadside}}^2 = \frac{B_{\mathrm{rms}}^2 r_{\mathrm{calibration}}^2}{S^2} e^{4\alpha_w r} \quad (11)$$

where $B_{\mathrm{rms}}$ is derived from the broadside beams (number 256 and 257) at the range, $r_{\mathrm{calibration}}$, equivalent to the depth of the P61 sample. Detailed information concerning the grain size distribution in suspension, $K_s$, is unknown and the calibration presented herein is based on the assumption that $K_s$ remains spatially and temporally constant. The mean of the recorded sound speed was 1474 m/s and the mean temperature of $19.9^0$ gives a value of $\alpha_w = 0.004$ Np/m derived using the formulae of Francois and Garrison (1982a and 1982b). The results obtained from the P61 samples are displayed in Fig. 5 and are plotted against $MK_S^2 K_{t,\mathrm{broadside}}^2$. The linear regression (dotted, $R^2 = 0.48$) of the total concentration (inverted triangles) in each sample and the linear regression (dashed and dotted, $R^2 = 0.57$) of the concentration greater than 62.5 μm (squares) are shown. As the intercept of the regression greater than

62.5 μm is closer to the theoretical intercept at the origin, the backscatter is reasoned to be dominated by the fraction greater than 62.5 μm. The fraction less than 62.5 μm (diamonds) remains reasonably constant for all seven samples with a standard deviation of ~1.5 % of the mean value, 0.219 g / L. A model is therefore adopted that assumes a constant wash-load component of 0.219 g / L and a suspended-load component that is uniquely related to the backscatter. The solid line in Fig. 5 shows the calibration derived by a least-squares fit through the origin of the fraction greater than 62.5 μm. Substituting the value of $K_{\mathrm{t,swath}}$ = $6.31 \times 10^{-7}$ counts $m^{3/2} s^{-1/2}$ obtained from the basin tests in to the gradient, $K_S^2 K_{\mathrm{t,broadside}}^2$, of the calibration fit gives a result of $K_s = 0.13$. This corresponds to a single-size grain radius in suspension of 160 μm using the form function expression of Moate and Thorne (2012) that was developed for generic application to sands of varying mineralogy with an assumed grain density of 2650 kg/$m^3$ based on the density of quartz. Although there is insufficient information regarding the suspended sediment grain size distribution to assess the accuracy of this estimate, it is a more realistic value for the location than the 2600 μm grain radius obtained by using the calibration constant derived from the results of Greenaway and Weber (2010) with $K_{\mathrm{t,swath}} = 3 \times 10^{-7}$ counts $m^{3/2} s^{-1/2}$.

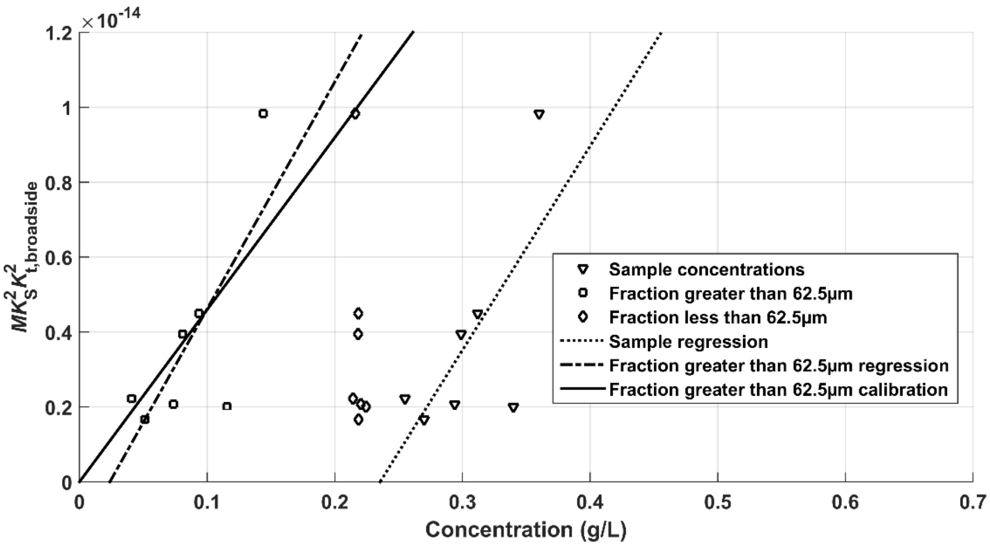


Figure 5 – Total water column sample concentrations and derived concentrations greater and less than 62.5 μm. Linear regressions of the total concentration and concentration greater than 62.5 μm are denoted by broken lines and the calibration through the origin are denoted by the solid line.

The mean of the seven calibrated, time-averaged, broadside MBES profiles is shown in Figure 6 over the range from the transducers to the bed at ~6.9 m below the flow surface. The results are derived by applying the value of $K_S^2 K_{\text{t,broadside}}^2$ from the calibration with Eq. (1) and the $\alpha_\text{S} = 0$ approximation. A value of $\alpha_w$ = 0.041 Np/m at the ADCP frequency is derived using the formulae of Francois and Garrison (1982a and 1982b) with the mean recorded temperature of $19.9^0$ C. As a comparison, the calibrated profile of the ADCP beam with the most similar range to the bed, beam 1, is also shown. The calibrated ADCP profile is processed using the same method, however the data were acquired after the MBES calibration and time-series were acquired. The near-field correction of Downing et al. (1995) is applied using a transducer diameter of 0.054 m to give values for $\psi_b$ in Eq.

(1). Despite the temporal offset and the spatial offset of the transducers and the 20 degree slant angle of the ADCP beam, there is a good agreement between the shape of the MBES and ADCP. This suggests that the sediment attenuation through the profile is relatively small, even at the 1200 kHz ADCP frequency and, critically, that the profiles are qualitatively similar beyond the range of 1.5 m where dynamic focusing is applied to the MBES receiver array. The results suggest that the expected near-field decrease in transmitted power close to the transmitter array is largely offset by the increase in beamwidth compared with the far-field and that an approximation of $\psi_b = 1$ is reasonable absent the existence of a near-field model and correction for a SeaBat 7125 MBES.

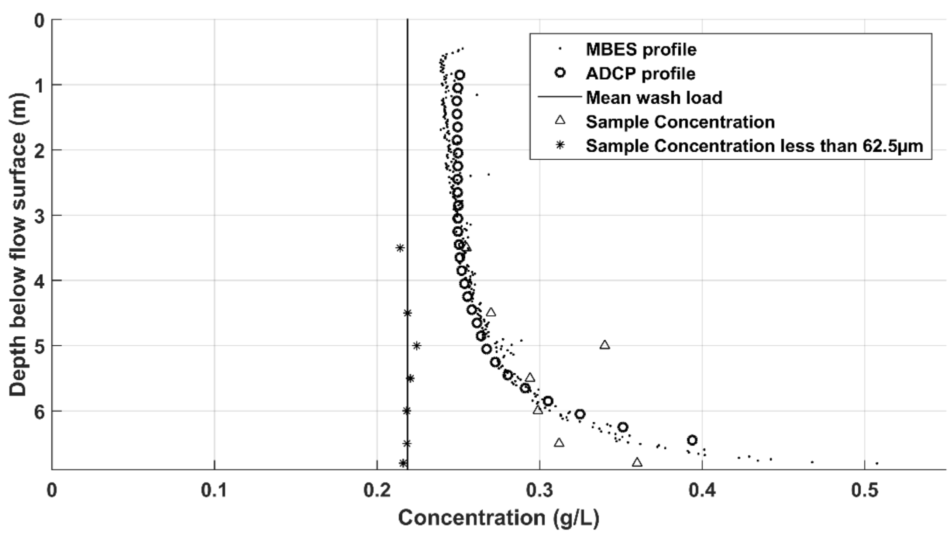


Figure 6 – Time-averaged vertical profiles of sediment concentration from the calibrated MBES broadside beams and ADCP beam.

The time-averaged backscatter data across the swath displayed noticeable artefacts along the direction of the beams in a radial pattern. Similar patterns were observed in the test basin at Blyth at higher ping repetition frequencies (20 Hz or greater) and were thought, therefore, to be attributable to surface reverberation. The location of the artefacts at the stationary dune site remained constant throughout the recording. However, water column backscatter recorded whilst the survey vessel was in motion showed the location of the radial artefacts changed constantly, reinforcing the surface reverberation explanation. Figure 7 shows the variation of the time-averaged, calibrated backscatter magnitude at a 2.8 m depth below the transducers for all beams relative to the broadside beams (numbers 256 & 257). It is assumed that the time-averaged concentration at that depth is constant across the swath and, therefore, that variations in magnitude are related to beam strength and surface reverberation. Smaller, superimposed ripples for beams ~1 to ~256 appear similar to those reported by Lanzoni and Weber (2010) who attributed them to interference from the 200 kHz projector.

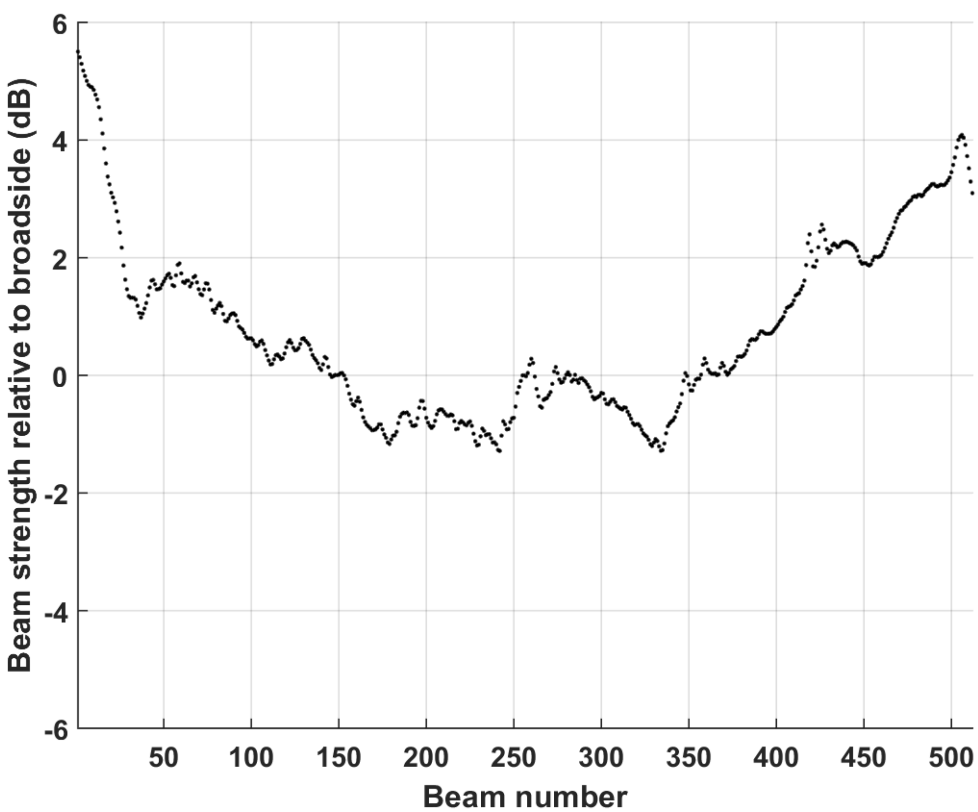

Figure 7 – Variation of the time-averaged backscatter magnitude at 2.8 m depth below the transducers for all beams relative to the broadside beams (numbers 256 & 257) after adjusting for spreading and attenuation losses.

Figure 8(a) shows the backscatter magnitudes from a single ping recorded at the field location. The echoes from the bed are clearly visible, as are the increased backscatter magnitudes from a plume of suspended sediment rising from the bed. Similar plumes were observed to advect with the flow from the left-side to the right-side of the swath throughout the recording. Figure 8(b) shows the same data after each beam is divided by the relative backscatter strength shown in Figure 7, calibrated to the water column samples and then spatially-averaged so that every averaged sample represents the root-mean-square of all the samples within a 0.19 m radius following the method presented in Simmons et al. (2010). The image demonstrates the two-dimensional suspended sediment flow field and the high spatial resolution that is capable from the data acquired in a single MBES ping.

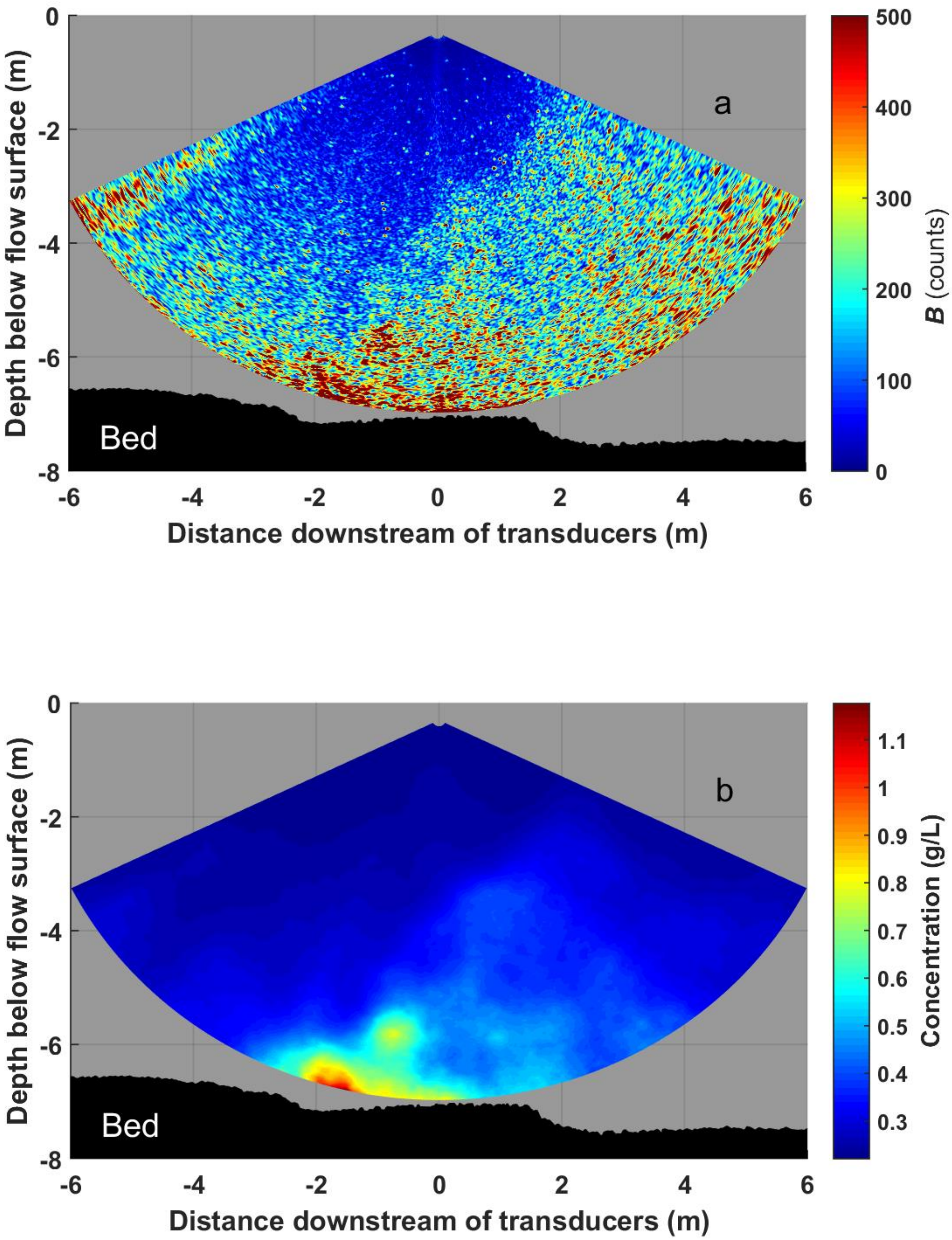


Figure 8 – (a) Magnitude data from a single ping collected over the lee-side of an alluvial sand-dune in the Missouri River at 396 kHz (outlier values above 500 counts are set to 500

counts on the color scale) and (b) the same data after calibration and two-dimensional spatial averaging.

Figure 9 shows a comparison between the concentration time series collected by (a) the MBES and (b) the ADCP over separate 100 s periods at the same field location. The MBES data were averaged over five beams around broadside (numbers 254 to 258) for each ping. The central beams on the 396 kHz and 512 beams equi-angle setting have a beamwidth of $0.54^0$ and a beam spacing of $0.25^0$. The five beams therefore cover an equivalent angle of $1.54^0$, roughly equivalent to the ADCP beamwidth of $1.4^0$, with a 46% overlap with the adjacent beam that leads to a marginal increase in the standard error compared with the value expected from Eq. (6). Further averaging over four successive pings increases the number of beams included in the average to 24 for the calibrated data displayed in Fig. 9(a). An approximately equivalent standard error is obtained for the ADCP data by averaging across 18 pings (three ensemble averages of six pings recorded by the instrument) to give the series shown in Fig. 9(b). The two time-series profiles have similar standard errors related to the random scattering of the sediment. However, for this example, the MBES data has a higher temporal resolution of 2.50 Hz compared with 0.57 Hz for the ADCP as a result of additional spatial averaging over five adjacent beams. The MBES also has a finer spatial resolution with sample spacing of 0.0214 m compared with 0.2 m for the ADCP. Furthermore, the MBES is capable of obtaining profile data much closer to the bed in the region where the ADCP is affected by side-lobe interference from the bed due to the beam's slant angle of $20^0$ to the vertical. This region is blanked out for the ADCP time-series in Fig. 9(b), whereas the range of the MBES series profiles in Fig.

9(a) extends to the penultimate bin prior to the largest return, giving a maximum distance above the bed of ~4 cm.

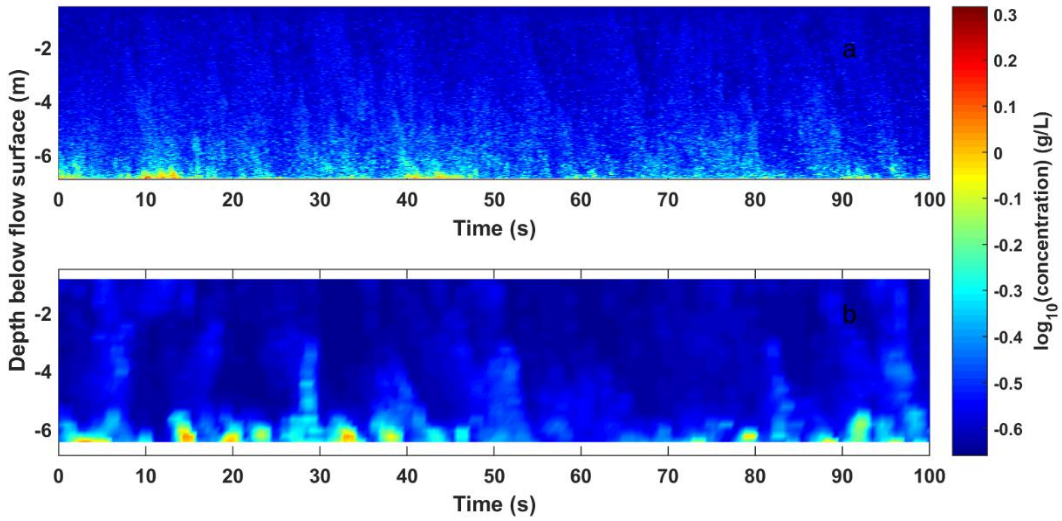


Figure 9 – Calibrated time series of (a) SeaBat 7125 multibeam data and (b) Workhorse ADCP data collected separately at the same location over a period of 100 s.

## 5. DISCUSSION

The primary objective of the research described herein was to evaluate the performance of an MBES system in a controlled test with known quantities of suspended material, and to relate these findings to the results of a field deployment of the system in a fluvial environment. The present paper has shown the clear potential of MBES for quantifying suspended sediment concentrations and visualizing such structures, and provided an analysis of the acoustic parameters that require attention in these applications.

The sensitivity of the SeaBat 7125 MBES system was evaluated by relating the cumulative backscatter from plumes of sand-sized sediment to the quantities of material released in to suspension during a controlled experiment in a calibration tank. The results of the calibration show a similar sensitivity for both 200 kHz and 396 kHz operating frequencies. The calibration constants enabled a model to be constructed of the effective operating range from the transducers for which the backscatter-to-noise ratio is likely to be greater than 0 dB for a range of sediment grain sizes and concentrations.

The field results demonstrate the ability of the MBES to image two-dimensional suspended sediment structures in the natural environment. However, reverberation effects were present in the data, suggesting the ping repetition frequency was set too high at 10 Hz for that particular location. Although a method was found to mitigate this distortion, an improved field methodology would incorporate an in-situ analysis of data recorded at different repetition frequencies to provide an estimate of the reverberation time. An analysis of the variation in backscatter strength and the sample fractions greater and less than a particle diameter of 62.5 μm demonstrated that the backscatter was dominated by the larger grain size fraction and that the wash load remained constant with depth. The backscatter model therefore treated variations in backscatter strength as variations in concentration above a constant wash load concentration. A comparison with time-averaged ADCP profiles acquired at the same location at a higher acoustic frequency show similar results, but the time-series concentration data clearly demonstrate the advantages of the MBES over the ADCP in terms of greater vertical and horizontal resolution and an ability to profile the water column closer to the bed where sediment transport rates are at their greatest. However, the horizontal extent of the near-bed samples in the 2D swath is limited to the beams with the shortest range to the bed due to the side-lobe interference arc.

It is suggested that future work should incorporate a calibration for the higher frequency instrument that is used in conjunction with the calibrated MBES and that grain size distributions are obtained from water column samples and bed samples. The combination of two calibrated instruments would enable an estimate of the mean grain size in the water column and would also enable a comparison of the temporal variation in backscatter strength between the MBES, in the grain size sensitive Rayleigh regime, and an ADCP/ABS instrument with a frequency in the megahertz range, where grain size variability is likely to be reduced depending on the relationship between the frequency and the mean grain size.

Data were recorded in the test basin for a range of settings of the transmitter power, receiver gain and pulse length but it was not possible to assess the linearity of the system settings as the backscatter from the bed was often clipped due to saturation. Such an evaluation, for a SeaBat 7125 MBES, has been reported by other researchers (Greenaway and Weber, 2010) using data obtained in a calibration tank and the bed-echoes from a field deployment. The system TVG was set during acquisition for both the basin tests and the field deployment under the assumption that the function is described explicitly by the formula in the user manual. However, the actual function used by the SeaBat 7125 and applied to the data herein differs from the formula in the manual and was supplied in commercial confidence. We therefore recommend that the TVG is not set during acquisition unless the formula has been supplied by Teledyne-RESON. Future work to accurately evaluate the combined axial near-field correction function of the transmitter and receiver, $\psi_b$, either through numerical modelling or by measurement in a calibration tank using a target sphere and hydrophone, would be valuable to further assess the accuracy of measurements within the near-field.

## ACKNOWLEDGEMENTS

This research was funded by the Natural Environment Research Council, UK, grant NE/D014530/1 to DRP and JLB. We are very grateful to Kevin Johnson of the USGS for his field assistance at different stages of this research and to the staff of the New and Renewable Energy Centre, Blyth, UK. Chris Malzone, John Fraser, and James Coleman of Teledyne-RESON provided technical support and information throughout the project for which we are extremely grateful.

## References


Best, J.L. **(1993)** "On the interactions between turbulent flow structure, sediment transport and bedform development: some considerations from recent experimental research". In: Turbulence: perspectives on flow and sediment transport, (Eds: Clifford, N., French, J.R. and Hardisty, J), 61-92. Wiley and Sons.

Best, J.L., Kostaschuk, R.A., Peakall, J., Villard, P.V. and Franklin, M. **(2005)** "Whole flow field dynamics and velocity pulsing within natural sediment-laden underflows". Geology, 33, 765-768.

Best, J., Simmons, S., Parsons D., Oberg. K., Czuba, J., and Malzone, C. **(2010)**. "A new methodology for the quantitative visualization of coherent flow structures in alluvial channels using multibeam echo-sounding (MBES)," Geophys. Res. Lett. **37**, L06405, doi:10.1029/2009GL041852.

Colbo, K., Ross, T., Brown, and Weber, T. **(2014)** "A review of oceanographic applications of water column data from multibeam echosounders," Estuarine, Coastal and Shelf Science **145**, 41-56.

Czuba, J.A., Best, J.L., Oberg, K.A., Parsons, D.R., Jackson, P.R., Garcia, M.H and Ashmore, P. **(2011)** "Bed morphology, flow structure, and sediment transport at the outlet of Lake Huron and in the upper St. Clair River". Journal of Great Lakes Research, **37**, 480-493.

Flood, R.D., Hiscott, and R.N., Aksu, A.E., **(2009)**. "Morphology and evolution of an anastomosed channel network where saline underflow enters the Black Sea," Sedimentology, **56**, 807-839

Fonseca, L., and Mayer, L. **(2007)**. “Remote estimation of surficial seafloor properties through the application Angular Range Analysis to multibeam sonar data,” Marine Geophysical Researches. **28**, 119-126

Francois, R. E., and Garrison, G. R. **(1982a).** "Sound absorption based on ocean measurements. PartI: Pure water and magnesium sulphate contributions", J Acoust. Soc. Am 72(3), 896–907.

Francois, R. E., and Garrison, G. R. **(1982b).** "Sound absorption based on ocean measurements. PartII: Boric acid contribution and equation for total absorption.", J. Acoust. Soc. Am. 72: 1879–1890.

Gaunaurd, G.C., and Uberall, H. **(1983)**. “RST analysis of monostatic and bistatic acoustic echoes from an elastic sphere,” J. Acoust. Soc. Am. **73**, 1–12.

Greenaway, S.F, and Weber, T.C., **(2010)**. “Test methodology for evaluation of linearity of multibeam echosounder backscatter performance,” Proceedings of the Oceans 2010 MTS/IEEE Seattle Conference and Exhibition, doi: 10.1109/OCEANS.2010.5664383.

Guy, H. P. & Norman, V. W. **(1970)**. Field methods for measurement of fluvial sediment. Book 3, Chapter C2, Page 59, Techniques of Water Resources Investigation of the US Geological Survey (US Govt Printing Office, Washington DC).

Hay, A.E. **(1983)**. “On the Remote Acoustic Detection of Suspended Sediment at Long Wavelengths,” J. Geophys. Res. **88**, 7525–7542.

Holdaway, G.P, Thorne, P.D., Flatt, D., Jones, S.E., and Prandle, D. **(1999)**. “Comparison between ADCP and transmissometer measurements of suspended sediment concentration,” Cont. Shelf Res. **19**, 421–441.

Kestin, J., Sokolov, M. and Wakeham, W.A., **(1978)**. "Viscosity of liquid water in the range -8$^0$C to 150$^0$C" J. Phys. Chem. Ref. Data, **7(3)**, 941-948.

Lane, S.N., Parsons, D.R., Best, J.L., Orfeo, O., Kostaschuk, R.A., and Hardy, R.J. **(2008)**. "Causes of rapid mixing at a junction of two large rivers: Rio Parana and Rio Paraguay, Argentina," J. Gephys. Res. **113,** F02024, doi:10.1029/2006JF000745.

Lanzoni, J.C., and Weber, T.C. **(2010)**. "High-resolution calibration of a multibeam echo sounder," Proceedings of the Oceans 2010 MTS/IEEE Seattle Conference and Exhibition, doi: 10.1109/OCEANS.2010.5664519.

Latosinski, F. G., Szupiany, R. N., García, C. M. Guerrero, M., and Amsler, M.L **(2014).** "Estimation of Concentration and Load of Suspended Bed Sediment in a Large River by Means of Acoustic Doppler Technology," J. Hydr. Eng. **140(7)** , 04014023.

Leeder, M. R. **(1983)**. "On the interactions between turbulent flow, sediment transport and bedform mechanics in channelized flows," Spec. Publ. Intern. Assoc. Sedimentologists **6**, 5-18.

Libicki, C., Bedford, K.W., and Lynch, J.F., **(1989)**. "The interpretation and evaluation of a 3-MHz acoustic backscatter device for measuring benthic boundary layer sediment dynamics," J. Acoust. Soc. Am. **85(4)**, 1501-1511.

Mills, B. Y., and Little, A. G. (**1953**). "A high resolution aerial system of a new type," Aust. J. Phys. **6**, 272–278.

Moate, B.D., and Thorne, P.D. (**2012)**. "Interpreting acoustic backscatter from suspended sediments of different and mixed mineralogical composition," Cont. Shelf Res. **46**, 67-82.

O’Neill, F. G., Simmons, S. M., Parsons, D. R., Best, J. L., Copland, P. J., Armstrong, F., Breen, M., and Summerbell, K. **(2013)**. “Monitoring the generation and evolution of the sediment plume behind towed fishing gears using a multibeam echosounder,” ICES Journal of Marine Science **70**, 892–903.

Parsons, D.R., Best, J.L., Orfeo, O., Hardy, R.J., Kostaschuk, R., and Lane, S.N. **(2005)**. “Morphology and flow fields of three-dimensional dunes, Rio Parana, Argentina: Results from simultaneous multibeam echo sounding and acoustic Doppler current profiling,” J Geophys. Res. **110**, F04S03, doi:10.1029/2004JF000231.

Parsons, D.R., Peakall, J., Aksu, A.E., Flood, R.D., Hiscott, R.N., Besiktepe, S, and Mouland, D. **(2010)**. “Gravity-driven flow in a submarine channel bend; direct field evidence of helical flow reversal, ” Geology **38**, 1063-1066

Schimel, A., Beaudoin, J., Gaillot, A., Keith, G., Le Bas, T., Parnum, I., Schmidt Val **(2015)**. “Processing backscatter data: from datagrams to Angular responses and mosaics”, In Lurton, X.; Lamarche, G. Backscatter measurements by seafloor-mapping sonars. Guidelines and Recommendations. A collective report by members of the GeoHab Backscatter Working Group. Geohab Report. 150p. Chap.6, 133-164. http://archimer.ifremer.fr/doc/00269/37977

Sheng, J., and Hay, A. E. **(1988)**. “An examination of the spherical scatterer approximation in aqueous suspensions of sand,” J. Acoust. Soc. Am. **83**, 598-610.

Shugar, D.H., Kostaschuk, R., Best, J.L, Parsons, D.R., Lane, S.N., Orfeo, S., and Hardy, R.J. **(2010)**. “On the relationship between flow and suspended sediment transport over the crest of a sand dune, Río Paraná, Argentina,” Sedimentology **57**, 252–272.

Simmons, S.M., Parsons, D.R, Best, J.L., Malzone, C., and Keevil G.M. **(2008)**. “Imaging of Large-Scale Sediment Transport Dynamics with Multibeam Sonar,” Proceedings of Acoustics '08 Paris. 9th European Conference on Underwater Acoustics, ECUA2008 Paris, France, European Acoustics Association, pp. 1907–1912.

Simmons, S.M., Parsons, D.R., Best, J.L., Orfeo, O., Lane, S.N., Kostaschuk, R., Hardy, R.J., West, G., Malzone, C., Marcus, J., and Pocwiardowski, P. **(2010)**. “Monitoring suspended sediment dynamics using MBES,” J. Hydr. Eng. **136**, 45–49.

Thorne, P.D., Agrawal, Y.C., and Cacchione, D.A. **(2007)**. “A comparison of near-bed acoustic backscatter and laser diffraction measurements of suspended sediments,” IEEE J. Ocean. Eng. **32**, 225–235.

Thorne, P.D., Hardcastle, P.J., and Soulsby, R.L. **(1993)**. “Analysis of acoustic measurements of suspended sediments,” J. Geophys. Res. **98**, 899–910.

Thorne, P. D., Hurther, D., Moate, B. D., **(2011).** “Acoustic inversions for measuring boundary layer suspended sediment processes,” J. Acoust. Soc. Am., **130 (3)**. 1188-1200.

Thorne, P.D., and Hurther, D. **(2014)**. “An overview on the use of backscattered sound for measuring suspended particle size and concentration profiles in non-cohesive inorganic sediment transport studies,” Cont. Shelf Res. **73**, 97–118.

Traykovski, P., Hay. A.E., Irish, J.D., and Lynch, J.F. **(1999)** “Geometry, migration and evolution of wave orbital ripples at LEO-15,” J. Geophys. Res. **104(C1)**, 1505–1524.

Urick, R.J. **(1948)**. “The absorption of sound in suspensions of irregular particles,” J. Acoust. Soc. Am. **20**, 283–289.

Vincent, C.E. **(2007)**. “Measuring suspended sand concentration using acoustic backscatter: a critical look at the errors and uncertainties,” in *Coastal and Shelf Sediment Transport*, edited by P. S. Balson and M. B. Collins (Geological Society of London, London), Vol. **274**, pp. 7–15.

Welton, B., **(2014)**. “A field method for backscatter calibration applied to NOAA's Reson SeaBat 7125 multibeam echo-sounders,”. Thesis (M.S.), University of New Hampshire, ProQuest, UMI Dissertations Publishing, 1525648, 1-120.